7 Molecular Chirality in Chiral Assemblies

7.1 Detection of Chirality

7.1.1 Descriptors of Chiral Centers

For historical reasons three different nomenclatures exist for molecules with chiral centers, such as the one depicted in figure 7.1. Unfortunately these three descriptors are not always concordant - actually they sometimes dissent.

The oldest nomenclature refers to a physical property of these molecules, discovered in 1848 by Pasteur on the sodium-ammonium-salt of tartaric acid[1]. He found that, upon illumination of chiral molecules with linearly polarized light, the polarisation plane was rotated. Depending on the direction of rotation, clockwise or counterclockwise, i.e. right or left, these molecules are described as $+$ or $-$. Using optical rotation, Pasteur was able to distinguish and manually separate the two enantiomers of sodium-ammonium-tartrate[199–202].

In 1874 Van't Hoff[203, 204] and Le Bel[205] independently developed the tetraeder model for carbon-based molecules, as shown in the stereo formula of figure 7.1. They proposed that, in order to obtain an energy minimum, the four ligands of a carbon atom have to be arranged in a tetrahedral fashion to observe ideal spatial separation. This model was the first model able to explain the structure of organic molecules and many of their properties. In such tetrahedron conformation, two possible arrangements of four different ligands can be realized. These mirror image conformations are not superimposable. In 1881 Emil Fischer performed experiments on the stereoisomers of monosaccharides [206, 207]. Based on the simplest carbohydrate, glyceraldehyde $OHC-CH(OH)-CH_2OH$, he developed a projection of these stereocenters and their ligands in one plane - the so called "Fischer projection", where the isomer-determining OH-group of glyceraldehyde was located either

[1]Historically the observable tartar was assumed to be the invisible tartaric acid. Only in 1769 the tartar was identified as the salt and the "real" tartaric acid was discovered by Scheele[198].

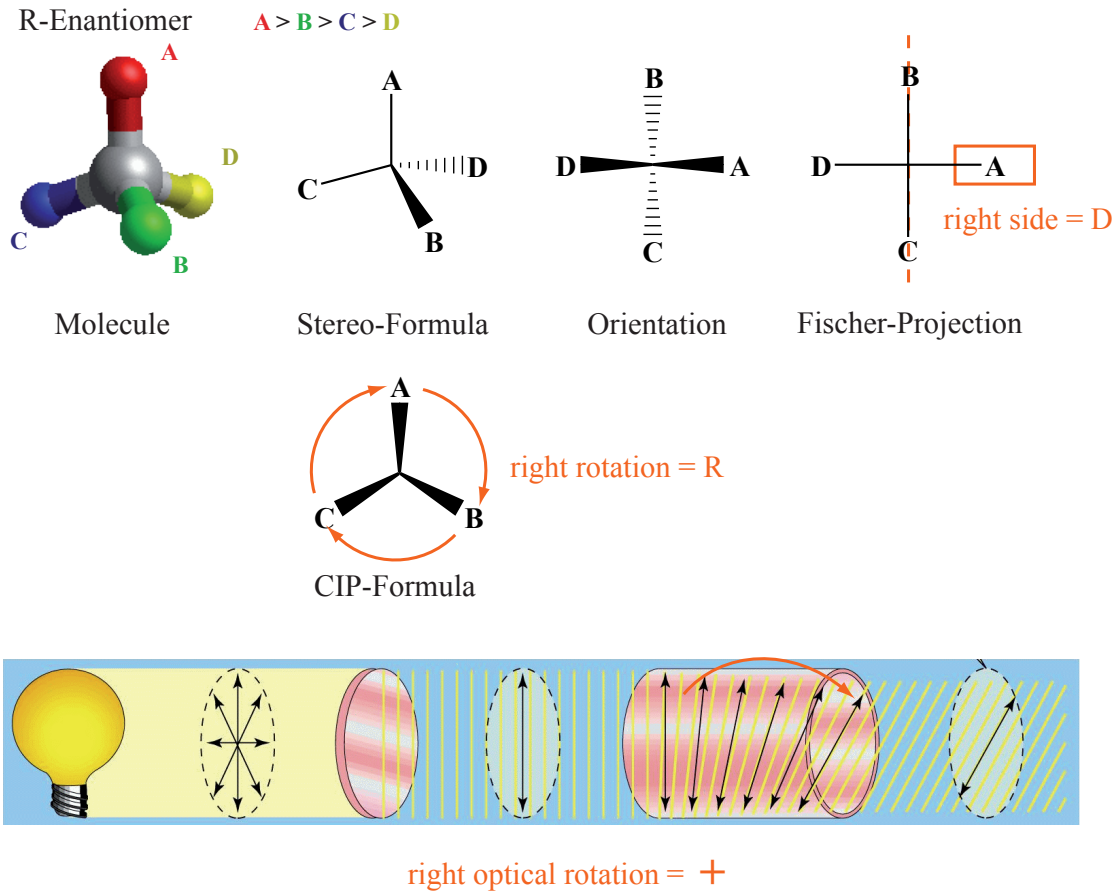

Figure 7.1: *Example molecule with a chiral center with the four different ligands A, B, C and D. Several methods exist to represent the molecular structure in a two-dimensional drawing. In the stereo-formula, lines represent bonds in the paper plane, the solid arrow represents a bond sticking out of the plane, the dashed arrow one, sticking into the plane, respectively. If the molecule is rotated in a fashion that two bonds show into the plane and two stick out, as shown in the "orientation" image, this conformation can be directly described by the "Fischer-projection". Horizontal bonds stick out of the plane, vertical ones into the plane. To achieve the representation determining the CIP-descriptor, the ligand of least priority D is turned into the plane. The inset in the bottom shows schematically the principle of optical rotation.*

on the right or on the left side of the molecular chain. Thus Fischer proposed a descriptor *D* (**d**exter (lat.) = right) or *L* (**l**aevus (lat.) = left), respectively. The descriptor of other chiral molecules is determined by their conformation in correlation to the glyceraldehyde molecule. The overall descriptor is given by the chiral center with the greatest distance to the *C*1 atom of the molecular chain. Fischer assigned the D-descriptor to the clockwise rotating (+)-glyceraldehyde, which in this case could be shown to be correct. Nevertheless there exist several molecules where the correlation that a *D*-molecule is also a +-molecule does not hold true.

As the Fischer nomenclature is only a relative nomenclature, an absolute one had to be developed, a task which was performed by Cahn, Ingold and Prelog in 1966[208]. In order

to describe a chiral center, the adjacent ligands are labeled A, B, C and D according to their chemical priority such as $A > B > C > D$, where the chemical priority is determined by the atomic number of the atom directly adjacent to the chiral center, e.g. $I > Br > Cl > S > P > F > O > N > C > H$. If two ligands have the same adjacent atom, the next atom is counted and so forth. This is known as the "sequence rule". Doublebonded atoms are counted twice, triple bonded atoms three times. The ligand D of least chemical priority is pointed into the paper plane as shown in the CIP-formula in figure 7.1. The appearance of the remaining ligands in decreasing order determines the chirality of the chiral center ("chirality rule"). Clockwise, i.e. right-handed, order is described as R (**r**ectus (lat.) = right), counterclockwise, i.e. left-handed, order as S (**s**inister (lat.) = left.). Every stereocenter within a molecule can thus be described in an absolute manner. Thus a molecule with e.g. two stereocenters can be either (R,R) or (S,S) or (R,S) (which is equivalent to (S,R)). While the first two forms are overall chiral ((R) or (S)), the latter form is an overall achiral molecule. A good example for such molecule is tartaric acid with its two stereocenters. As the CIP-nomenclature is the only absolute description of chiral centers, correlations to the other nomenclatures, i.e. an R-molecule is a D-molecule or an R-molecule is a +-molecule, are only valid in some exemplary cases. The properties of adsorbed chiral molecule, such as tartaric acid, alanine and cysteine, and the relation between their handedness (R or S) and optical rotation (+ or −) will be studied later in chapter 7.

7.1.2 Chirality Index

Up to now the description of chirality has been a mere phenomenological and qualitative one. For spectroscopy a quantitative description of chirality is of interest. Such models would allow the prediction of spectroscopic effects due to the molecular handedness. Since the discovery of chirality, theoretical models have been sought, the first one in 1890 by Guye[209, 210]. He defined a chirality product P for a chiral carbon center, where the four ligands describe the corners of a tetrahedron (i.e. the angle between every ligand would be the tetrahedral angle). When d_i are the distances of the center of mass of each of the six tetrahedral planes defined by each of the edges and the chiral center, P would be

$$P(d) = \prod_{i=1}^{6} d_i \ .$$

But only in the past years models have been developed, that indicate that a quantitative description of chirality might be possible. Still these theories have not yet been fully approved by experiment.

In 1970 Ruch and Schönhofer have developed a mathematical description of chirality[211].

Based on the observation of optical activity they proposed chirality functions describing the transformation behavior of several molecule classes. These chirality functions were based on group theory could only be used using several approximation operations. Another approach by Luzanov and Babich was the utilization of first principles calculations and the definition of an electronic and topological chirality operator[212].

In the 1990s Mislow and coworkers developed a differ mathematical expression for the quantification of chirality based on Guye's work. They investigated the triangle described by the three high-priority ligands (compare figure 7.1)[213] and found for P

$$P = (a - b)(b - c)(c - a) \ , \tag{7.2}$$

where a, b and c are the three sides of the triangle. They evaluated this expression that far, that they could describe the most chiral tetrahedron, which has least overlap with its mirror image tetrahedron.Up to now this model can only be applied to geometrical figures and not to real molecules[213].

In the style of the mathematical derivations by Ruch[211], Capozziello and Lattanzani developed a simple geometric and algebraic approach to describe the behavior of molecules containing chiral centers[214–217].

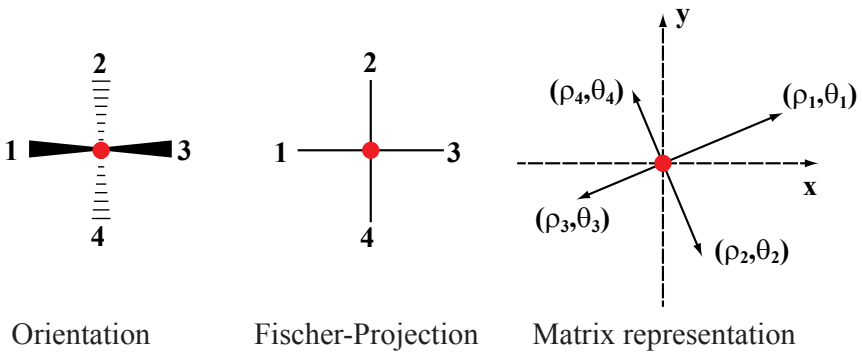

Figure 7.2: *A stereocenter (red), whose orientation is shown on the left, can be represented by a Fischer projection. In this projection each ligand* 1 *to* 4 *(independent of priority) can be described by its length* ρ *and its angle toward the main coordinate system* θ*.*

As shown before any molecule with a stereocenter and four ligands 1 to 4 (neglecting the priority A to D) can be described by the Fischer projection in the x, y-plane. If the stereocenter is chosen as the origin of the plane, each ligand can be described by its length ρ and its relative position toward the axis θ using a rotation versus. I.e. each ligand j is described by the parameter pair $\{\rho_j; \theta_j\}$ and the vector $\Psi_j = \rho_j e^{i\theta_j}$ (i is the imaginary number $i = \sqrt{-1}$). The whole molecule can then be described by

$$M = \sum_{j=1}^{4} \Psi_j = \sum_{j=1}^{4} \rho_j e^{i\theta_j} \ . \tag{7.3}$$

By definition two molecules are chiral if they are not superimposable. This can be reached by inversion of any two bonds in the projection plane in figure 7.2, e.g. inversion of ligand 1 with ligand 3. Or, in other words, one inversion has to be made to make the two enantiomers with one stereocenter superimposable. This is described by the chirality number

$$\chi = \{n, p\} \ , \tag{7.4}$$

with n the number of stereocenters in the molecule and p the number of inversions needed to reach superimposability. Starting from one stereocenter Capozziello and Lattanzani showed, that one can subsequently add additional stereocenters along the molecular chain and determine n and p for each with $0 \leq p \leq n$, following an "Aufbau" principle[217]. Then the relationship between two chiral molecules is directly accessible by χ. For achiral molecules $\chi \equiv \{n, 0\}$, for diastereomers $\chi \equiv \{n, p < n\}$ and for enantiomers $\chi \equiv \{n, n\}$.

The molecular descriptor M can also be seen as a column vector

The Fischer projection shown in figure 7.2 is chosen as the fundamental projection which can be represented by a 4×4 operator

$$\chi_1 = \begin{pmatrix} 1 & 0 & 0 & 0 \\ 0 & 1 & 0 & 0 \\ 0 & 0 & 1 & 0 \\ 0 & 0 & 0 & 1 \end{pmatrix} \ , \tag{7.5}$$

which is the identity matrix. Starting from this representation, every other projection can be reached by application of the specific operator χ_j onto M. All operators are given in literature[217]. All χ give the group $O(4)$ with two subgroups with determinants $+1$ and -1 representing the two enantiomers.

Basak and coworkers[218] finally developed a system to numerically characterise chirality based on the CIP-nomenclature. Upon aligning the molecule according to the CIP-rules with the ligand of lowest priority into the rear, the three ligands of highest priority are viewed from a reference point. For every atom k in each group $i = a, b, c, d$ a valence delta value δ_i^v is assigned according to the method of Hall and Kier[219] from

$$\delta_k^v = \frac{(Z_k^v - H_i)}{(Z_k - Z_k^v - 1)} \ , \tag{7.6}$$

with Z_k being the number of electrons in atom k, Z_k^v the number of valence electrons in atom k and H_k the number of hydrogens attached. For each group i the δ-value is calculated as follows.

$$\delta_i^v = \delta_{n1}^v + \frac{\delta_{n2}^v}{2} + \frac{\delta_{n3}^v}{4} + \frac{\delta_{n4}^v}{8} + \dots \ . \tag{7.7}$$

From these group-δ-values the relative chiral indices RCI can be calculated for one chiral centeres RCI can be calculated for one chiral center

$${}^V RCI_R = \delta_a^v + (\delta_a^v + \delta_a^v\delta_b^v) + (\delta_a^v + \delta_a^v\delta_b^v + \delta_a^v\delta_b^v\delta_c^v) + \delta_a^v\delta_b^v\delta_c^v\delta_d^v \ , \tag{7.8}$$

$${}^V RCI_S = \delta_a^v + (\delta_a^v + \delta_a^v\delta_c^v) + (\delta_a^v + \delta_a^v\delta_c^v + \delta_a^v\delta_b^v\delta_c^v) + \delta_a^v\delta_b^v\delta_c^v\delta_d^v \ , \tag{7.9}$$

and for molecules with N chiral centers

$${}^V RCI = \sqrt{\frac{1}{N}\sum_{i=1}^{N}({}^V RCI_i)^2} \ . \tag{7.10}$$

Instead of the valence connectivity V also the formula weights W or the electrotopological state I can be used to calculate the δ and subsequently the RCI values.

These RCI values can be used to identify the relative importance of stereocenters and provide a hint on the absolute handedness of the molecule.

7.1.3 Optical Activity and Circular Dichroism

As mentioned above chiral molecules exhibit the physical property of optical activity or optical rotation, i.e. the rotation of the polarization plane of linear polarized light through chiral molecules and may be used to distinguish the different isomers[220].

Several theoretical models for the explanation of this phenomenon exist[221, 222]. In a simple and approach, linear polarised light can be envisioned as a superposition of left- and right-circular polarised light of identical amplitude and phase $E_R = E^+$ and $E_L = E^-$ as shown in figure 7.3. These two components can be expressed as

$$E^{\pm} = E\ \hat{i}\ cos\Phi_{\pm} \mp E\ \hat{j}\ sin\Phi_{\pm} \ , \tag{7.11}$$

with $\hat{i}$ and $\hat{j}$ are the unit vectors perpendicular to the light propagation direction. $\Phi_{\pm}$ can be expressed in terms of time, location along the propagation axis z and light frequency ν (c is the speed of light).

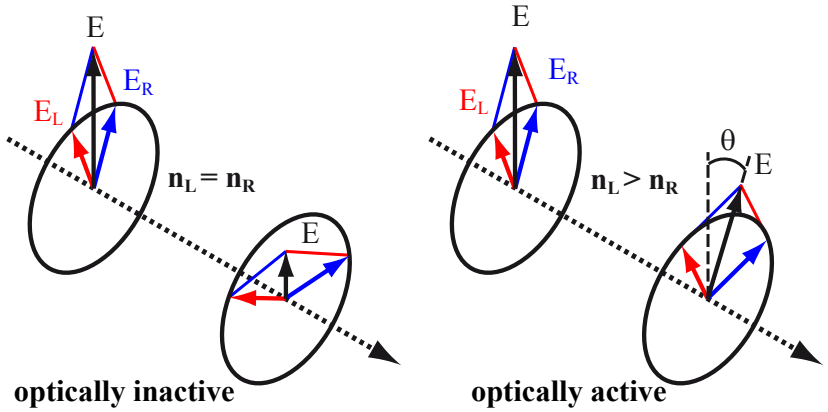

Figure 7.3: *Addition of differently absorbed right and left circular polarized light leads to elliptical polarized light.*

$$\Phi_{\pm} = \omega t - 2\pi z/\lambda_p m \tag{7.12}$$

$$\omega = 2\pi\nu \tag{7.13}$$

$$1/\lambda_{\pm} = n \pm \nu/c \ . \tag{7.14}$$

The optical active medium surpassed is characterised by the refractive index$n$, which can be decomposed into a left and right handed term n_- and n_+

$$n = 0.5 \cdot (n_+ + n_-) \ . \tag{7.15}$$

The difference between the two refractive indices is given as $\Delta n = n_+ - n_-$, such ases is given as $\Delta n = n_+ - n_-$, such as

$$\Phi_{\pm} = \omega t - n_{\pm} - \omega z/c \tag{7.16}$$

$$= \Phi \mp (\omega z/2c)\Delta n \ , \tag{7.17}$$

with $\Phi = \omega t - n\omega z/c$.

In an achiral medium, i.e. a medium that does not exhibit optical activity $\Delta n = 0$ and $E^{\pm} = E\ \hat{i}\ cos\Phi \pm E\ \hat{j}\ sin\Phi$. The superposition of E^+ and E^- gives the overall electric vector of the light beam

$$E = E^+ + E^- = 2E\ \hat{i}\ cos\Phi \ . \tag{7.18}$$

As the two polarisations are like enantiomers to each other, their interaction with enantiomorphous matter, i.e. chiral molecules, is different. Due to different refractive indices $n_l = n_-$ and $n_r = n_+$ in the left and right-handed molecule the velocity of propagation for left- and right-circular polarized light is changed. This results in an overall rotation of the polarization plane by an angle

$$\theta = (\omega z/2c)\Delta n \ . \tag{7.19}$$

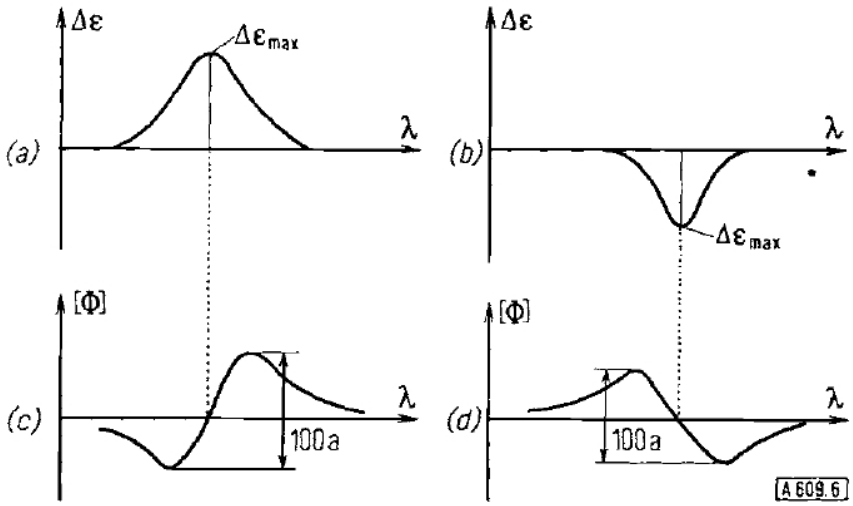

Figure 7.4: *Positive (a) and negative (b) CD with corresponding ORD partial curves (c) and (d)[223].*

The wavelength dependent detection of θ is known as optical rotatory dispersion (ORD)[223]. For $n_L > n_R$ (i.e. $\Delta n > 0$) $\theta > 0$ and the polarisation plane is rotated to the right. The molecule is denotes as dexrotatory, described by the symbol $+$. A laevorotatory molecule has negative optical activity $-$, the polarisation plane is rotated to the left, i.e. $\theta < 0$ because of $n_L < n_R$ (i.e. $\Delta n < 0$).

The ORD is especially strong and changes the sign at specific absorption bands of the chiral medium. This effect is known as Cotton Effect, its descriptive sign depending on the change of sign at the absorption band maximum.

The different geometry of two enantiomers at the chiral center leads to a variation in the spatial extension of the electromagnetic field over the molecule. According to Maxwell's equation[222] the spatial variation of the electric field E is proportional to the time variation of the magnetic field B. Therefore the part of the electric polarization P induced by the spatial variation of E can also be expressed by the time variation of B

$$P = N\alpha E - N\beta\dot{B} \tag{7.20}$$

with α and β being some constants, N is the density of molecules. Initially B is perpendicular to E. Thus the E component induces a dipole in the plane of the electric field, but the B component a a dipole perpendicular to it and thereby an oscillating field in the same plane is produced. The superposition of both fields give a electric field plane rotated with respect to the original one. Solving Maxwell's equation for equation (7.1.3) gives

$$\Delta n = \frac{2\omega\beta N}{c\ \epsilon_0}\ , \tag{7.21}$$

where ϵ_0 is the vacuum permittivity, that is defined by the speed of light c and the vacuum dipole moment μ_0 following $\epsilon_0\mu_0 = 1/c^2$. Using equation (7.19) the optical rotation angle θ of light passing an active medium over the length can be determined with

$$\theta = \beta\ \mu_0\ \omega^2\ N \cdot l\ . \tag{7.22}$$

This equation shows some very fundamental proportionalities for the optical rotation, the dependence on the length l, the frequency of the light ω, the density N and the coefficient β that can be seen as the molecule intrinsic property. An expression for β can be analytically derived using Maxwell's equation. This leads to the so called Rosenfeld equation[222]

$$\theta = nl(2\mu_0/3\hbar)\sum_n \left(\frac{\omega^2 R_{n0}}{\omega_{n0}^2 - \omega^2}\right)\ , \tag{7.23}$$

where the rotational strengths R_{n0} of the transition from the ground state into state n is introduced as the determining factor for θ

$$\theta \propto \sum_n R_{n0}\ . \tag{7.24}$$

This rotational strength is given by

$$R_{0n} = Im(\mu_{0n} \cdot m_{0n})\ , \tag{7.25}$$

the imaginary part of the product from μ_{0n}, the electric dipole operator, and m_{0n}, the magnetic dipole operator of the transition from the ground state to the state n. This is in analogy to equation .

If $\mu_{0n} = 0$, because no light is absorbed, no optical rotatory dispersion and also no circular

dichroism can occur.

The electric dipole operator results in a charge separation, the magnetic dipole operator in charge circulation. The combination of the two results in a charge separation and circulation along a screw axis. For a symmetrical molecule there will be no preferred direction for the charge circulation, and R_{0n} will be zero. If μ_{0n} and m_{0n} are orthogonal, R_{0n} will also be zero.

Also the extinction coefficient differs for each handedness. Thus the absorption of the two polarisations is different resulting in two waves of different amplitude. Superposition leads to elliptical polarised light or in the extreme case, if one component is totally absorbed, to opposite circular polarised light. This effect, known as circular dichroism (CD)[223] is usually very small except at the absorption frequencies of the active medium. The circular dichroism can be expressed in analogy to the optical rotation by the difference of the extinction coefficients ϵ_L and ϵ_R

$$\Delta\epsilon = (\epsilon_L - \epsilon_R) \ . \tag{7.26}$$

Utilizing again the scheme depicted in figure 7.3 the angle θ can be described as follows

$$tan\theta = \frac{E_R - E_L}{E_R + E_L} \ , \tag{7.27}$$

where $E_L = E_-$ and $E_R = E_+$ are the vectors shown on the right after transition through an optically active medium.

For small angle θ, $tan\theta \approx \theta$ holds true. Since the measured light intensity $I = E^2$ equation 7.27 can be rewritten as

$$\theta(radians) = \frac{I_R^{0.5} - I_L^{0.5}}{I_R^{0.5} + I_L^{0.5}} \ . \tag{7.28}$$

Application of Lambert Beers Law in logarithmic form

$$I = I_0 e^{-A \ ln10} \ , \tag{7.29}$$

with A being the absorbance, and subsequent conversion of *radians* into *degrees* leads to

$$\theta = \Delta A \left(\frac{ln10}{4}\right) \left(\frac{180}{\pi}\right) \ , \tag{7.30}$$

where the difference in absorbance ΔA is described according to the Lambert-Beer law as

$$\Delta A = (\epsilon_{LCP} - \epsilon_{RCP}) \cdot n \cdot l \ . \tag{7.31}$$

This difference in absorption of left and right handed polarised light in a chiral medium is known as circular dichroism.

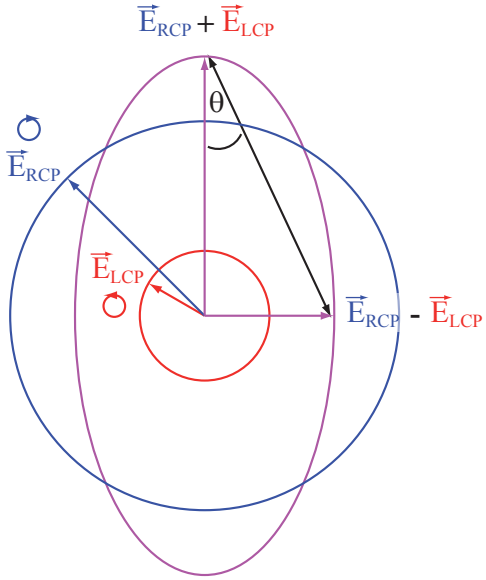

Figure 7.5: *The different absorption of left and right handed circular polarised light leads to an elliptical polarisation of previously linearly polarised light after surpassing a chiral medium[221].*

Again assuming linear polarised light as the superposition of left and right handed circular polarised light, this means that, after surpassing the chiral medium, the intensities of both polarisations are different from each other, as depicted in figure7.5[221]. The superposition of two circular polarisations with different intensities leads to elliptical polarised light. This is the phenomenology observed for circular dichroism.

Circular dichroism as described above is based on the detection of changes in circular polarised light after absorption through a chiral (liquid) medium, i.e. after light induced optical transitions within the molecules. UV or even x-ray light instead cause electronic transitions and even photoionization.

Dubs and coworkers showed that the angle resolved spectroscopy of photoelectrons excited with circular polarized light also exhibits a dichroism which is dependent on the alignment of the initial state[224–227] - circular dichroism in photoelectron angular distributions (CDAD). In early CDAD work strong spin-orbit coupling and high multipole interactions were assumed as origin of the effect. In the detection scheme as shown in figure 7.6 dichroic effects can be predicted already from the electric dipole approximation. Indispensable for the existence of CDAD is an alignment of the photon target states. A state with the total angular momentum J is defined as "aligned", if the magnetic sublevels M_J are not

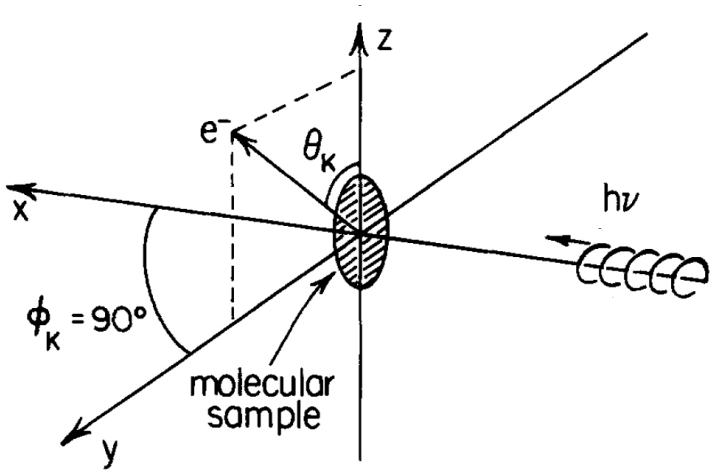

Figure 7.6: *Detection scheme for circular dichroism, displaying the coordinate system with respect to the photon source and the detection direction. – Figure reproduced from [224–227].*

uniformly populated. In contrast to "oriented" states, where the M_J are also nonuniformly populated, for alignment the M_J and $-M_J$ states have to be equally populated[2]. The alignment of this state in the experimental framework may have different origins: either the experimental setup is set up as shown in figure 7.6, where the non-coplanarity of excitation source, sample and detector creates a handed environment, or the molecular intrinsic chirality.

For an aligned state, the electric dipole moment is

$$D_0 = \left(\frac{4\pi}{3}\right)^{1/2} \sum_s r_s Y_{10}(\hat{r}_s) \ , \tag{7.32}$$

where r_s is the magnitude of the position vector $\hat{r}_s$ of the sth electron and Y is a spherical function.

This representation is within the coordinate system of the ionizing photon and has to be transformed into the experimental framework yielding in a much complex term for D_{μ_0}. Evaluation of this term, as can be found in literature[224–227], leads to an expression for the intensity I

$$I(\theta_k) \propto Y_{11}(\theta_p, \Phi_p) \sum_L F_L \ Y_{L-1}(\theta_k, \Phi_k) \ , \tag{7.33}$$

with Y again being spherical functions and F_L a factor.

[2]Aligned and oriented states give dichroic effects. Absorption of a linearly polarized photon creates an aligned state from an isotropic initial state, absorption of a circular polarized photon an oriented state[226].

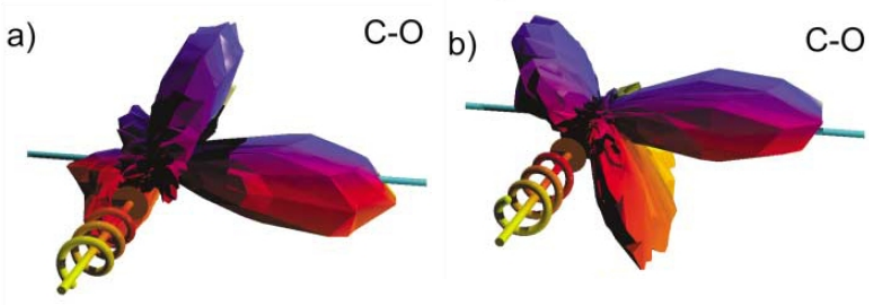

Figure 7.7: *Angular distributions of C1s photoelectrons from a CO molecule by absorption of left and right circularly polarized light (rotation of the polarization vector is indicated)[228]. The molecule is aligned along the z axis, with the carbon atom at negative z. – Figure reproduced from [228].*

In the laboratory framework the photon direction is (θ_p, Φ_p) and the electron collection plane is given by the angle (θ_k, Φ_k), (θ_p, Φ_p) is usually fixed, e.g. in form of the beamline. If (Φ_k) is fixed in a way that it is not coplanar with sample and excitation direction, then this geometry is inducing a framework in which an alignment can take place. This leads to CDAD-effects of intrinsic achiral molecules. A nice example has been reported by Dörner and coworkers, who investigated the CDAD effect in aligned CO and N_2 gas phase molecules[228]. The emission cones from the photoelectrons are shown in figure 7.7. The asymmetry in emission is clearly visible.

In the experiments of this thesis (Φ_k) was chosen to be coplanar and the CDAD observed in dependence of (θ_k) is due to the molecular chirality. The four different ligands around the chiral center prepare a nonisotropic state. The strength of the four ligands is described by a chirality index c_L as explained before (chapter 7.1.2) (P_L are Legendre polynomials)

$$I(\theta_k) \propto \sum_L c_L P_L^1(cos\theta_k) \ . \tag{7.34}$$

This is in close analogy to the general description for the angular distribution of emitted photoelectrons

$$I(\theta) = \sum_L b_L P_L(cos\theta) \ , \tag{7.35}$$

where P_L are Legendre polynomials, b_L coefficients and θ the angle between photon incidence and electron emission direction. From this starting point Ritchie developed an expression for the CDAD emitted from optically active molecules[229, 230], which was later on adapted by Hergenhahn and coworkers[231]. He showed that the emission follows a $A \pm B\ cos\theta + C\ cos^2\theta$ law, where A, B and C are coefficients.

While the beforehand description is based on a factorization of the spherical functions Y, Schönhense and coworkers[232–234]proposed a model based on symmetry adapted wave functions. These wave functions are no longer spherical and the symmetry of the Y functions is broken. This symmetry breaking is then the cause for CDAD.

The photoelectron intensity for a transition from the bound initial state $\Psi_i = \Psi_{n,l,j}$ into the free final state $\Psi_f = \Psi_{E_{kin},k}$ is

$$I(\vartheta, \phi) = c_\sigma |\vec{\epsilon}\langle \Psi_f | \vec{r} | \Psi_i \rangle^2 \ , \tag{7.36}$$

where $\vec{\epsilon} = \begin{pmatrix} \epsilon_x \\ \cdot\epsilon_y \\ \epsilon_z \end{pmatrix}$ is the polarisation vector (x and y component real, z component imaginary) For circular polarised light only ϵ_y is complex, the $x-$ and z-component real.

Assuming the circular polarised photon incidence to be in the x,z-plane under an angle α, the polarisation vector is

$$\vec{\epsilon} = \sqrt{1/2} \begin{pmatrix} cos(\alpha + \pi) \\ \\ -sin(\alpha + \pi) \end{pmatrix} \ . \tag{7.37}$$

To accurately determine now the CDAD, the wave functions $\Psi_{fi}^{x,y,z}$ have to be chosen symmetry adapted. An overview of those is given in literature[233].

Now the $I_{CDAD} = I^{i+} - I^{i-}$ can be constructed from a normal incidence (NI) term at $\alpha = 0$ and a grazing incidence (GI) term at $\alpha = \pi/2$

$$I_{CDAD} = cos(\alpha) \cdot I_{CDAD}^{NI} + sin(\alpha) \cdot I_{CDAD}^{GI} \ . \tag{7.38}$$

In all these descriptions the circular dichroism is based on the change of handedness in one of the "components" involved in the experiment. A CDAD experiment contains

- the handedness of the light (i.e. polarisation)
- the handedness of the measurement geometry
- the handedness of the molecules (i.e. chirality)

The change of handedness in any of these components can be seen as a parity operation changing the sign of the observed circular dichroism. That means, if the handedness of the photons and the molecular chirality are changed simultaneously, no change in circular dichroism can be detected.

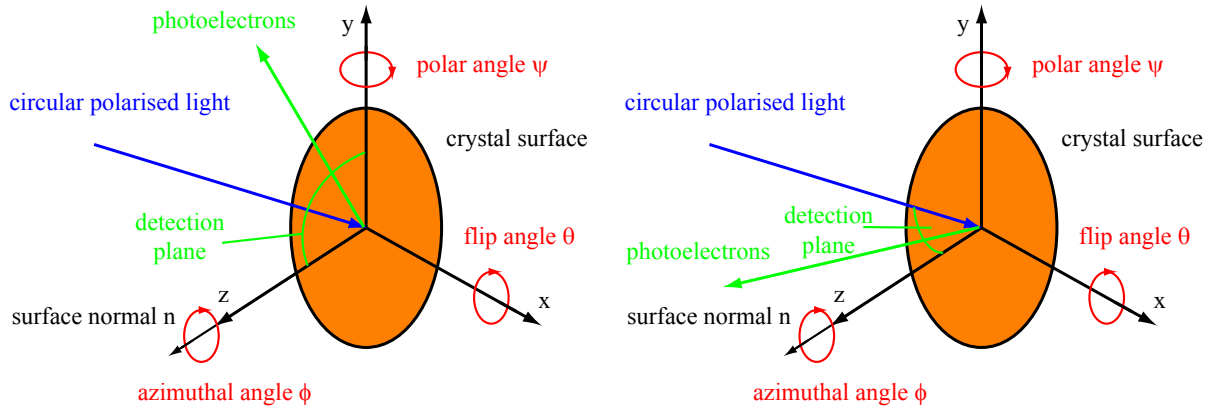

(a) *Experimental chirality.* **(b)** *No experimental chirality.*

Figure 7.8: *Two possible experimental geometries used for CDAD measurements. In (a) the geometry used e.g. by Schönhense and coworkers[232] is depicted. Here the x-z-plane is a mirror plane inducing an inherent experimental chirality. CDAD in dependence of the flip angle θ can be observed, intensity modulated in dependence of the azimuthal angle ϕ but independent of ψ. In (b) our experimental geometry is depicted. Here all measurements take place only within the x-z-plane, and thus no experimental geometry exists. The detected CD in dependence of the polar angle ψ cannot result from the experimental geometry.*

Obviously the experimental geometry plays a crucial role for the origin of the detected CDAD-effect. In an experimental geometry, as shown in figure 7.8a, where the photoelectrons are detected at an off angle from the plane defined by surface normal and light incidence beam, a CDAD in dependence of the angle θ can be detected. Here the x-z-plane represents a mirror image defining the handedness of the experimental setup. Such a setup is used by Schönhense and coworkers[232], Woodruff and coworkers[235] or is referred to in the work of Dubs and coworkers[225, 227]. In this context it has to be mentioned, that the angle θ is in literature sometimes referred to as "polar angle". Here this is the "flip angle", the "polar angle"-dependence of the CD signal that will be shown in this work refers to the polar angle ψ indicated in figure 7.8. Figure 7.8b shows the experimental geometry used in this work. Here incidence light, surface normal and photoelectron emission take place within the previously mentioned mirror plane. Thus no experimental handedness exists. A CDAD signal with dependence on the polar angle ψ has its origin in the sample under investigation, here the chiral molecules. The angles θ and ϕ are kept constant. Actually Venus, Kuch, Kirschner and coworkers reported on a CDAD signal in valence band emission from a clean Cu(110) upon change of the azimuthal angle ϕ, which they refer to as magnetic dichroism[236, 237]. This effect can be neglected here, as ϕ is kept constant throughout the experiments shown in this work.

Such a detection scheme as shown in figure 7.8b have previously been used by Piancastelli, Kim, Horn and coworkers for the investigation of adsorbed chiral molecules[238]. For butanediole adsorbed on Si(100) a circular dichroism signal in the emission from the C1s

core level could be detected for the chiral enantiomers, while the achiral isomer observed no such effect. The investigations on tartaric acid, shown later in this work are based on the preceding work of Kim and coworkers in this group.

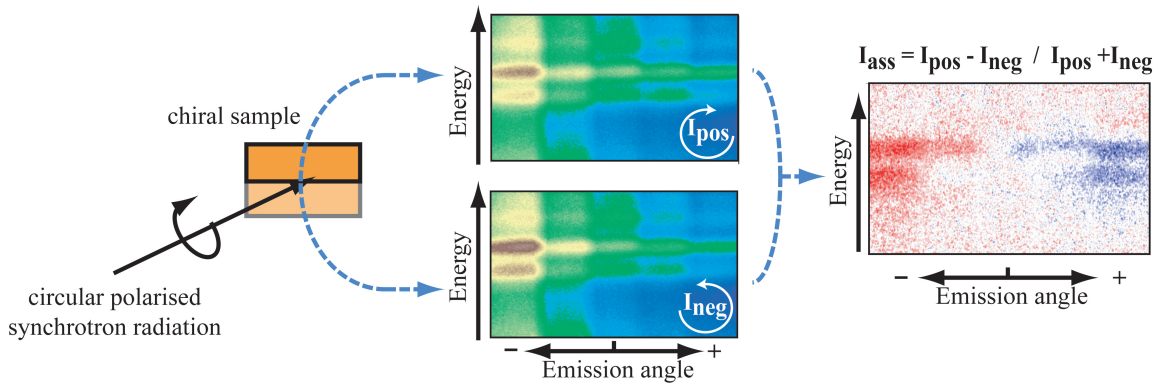

Figure 7.9: *For the detection of circular dichroism C1s core level spectra were acquired over a broad emission angle range, i.e. 20° around normal emission, using the imaging mode of the detector with circular polarised light. Two angle-resolved core level spectra for left- and right-circular polarised light, $I_{LCP} = I_{pos}$ and $I_{RCP} = I_{neg}$, were obtained. The asymmetry was calculated from these spectra with $I_{ass} = (I_{pos} - I_{neg})/(I_{pos} + I_{neg})$.*

In order to determine the angular dependence of the C1s-CD, core level spectra are obtained for a polar angle of normally ±20° around normal emission (NE). Using the imaging mode of the CCD-detector, slabs of 14° angular width with an overlap of about 4° are acquired with both left circular polarized light and right circular polarized light. This technique has previously been described by Kim, Horn and coworkers[238] who acquired single line scan spectra. For a more detailed analysis the acquisition over a wide angle range as done here is of advantage.

The resulting images are normalized to ring current, acquisition dwell time and samples taken, resulting in two C1s image maps I_{pos} and I_{neg} as shown in figure 7.9. For angles negative to normal emission, i.e. in direction of further grazing incidence, intensities increase due to the increased size of the grazing synchrotron spot. For further data clarification a two dimensional 3rd order polynomial fitted to the background regions of the maps, is subtracted. From these image maps the asymmetry plot is calculated following the equation

$$I_{ass} = \frac{I_{pos} - I_{neg}}{I_{pos} + I_{neg}} , \tag{7.39}$$

as shown in figure 7.9.

7.2 Chirality of Tartaric Acid

7.2.1 Adsorption of Tartaric Acid on Cu(110) - Chiral and achiral adsorption phases

Tartaric acid is without doubt one of the "drosophila" in the investigation of chiral surfaces. This is not gratuitous as tartaric acid on Raney nickel is actually one of the few effectively working heterogeneous chiral catalysts in industry.

The most popular appearance of tartaric acid is as tartar, i.e. the potassium salt of tartaric acid that appears at the bottom of wine bottles. Investigating these molecules Pasteur observed the phenomenon of optical activity and chirality.

A natural appearance of (the (R,R)-enantiomer of) tartaric acid is e.g. in wine, dandelion, sugar beets, black pepper and pineapple. Tartaric acid can be synthesized by the oxidation of calciumtartrate with sulfuric acid. It finds common use as antidegradant E334 in food and as binding agent in cement and plaster. Due to its ability to form metal complexes it is often used as chemical reagent, especially as an asymmetric catalyst for chiral synthesis.

The two stereocenters in the tartaric acid backbone give rise to the three isomers shown in figure 7.10. The possible (S,R)-isomer (not shown) can be transformed into the (R,S)-form by rotation and is thus equivalent to the latter one. The Fischer nomenclature and optical rotation properties are given in table 7.1.

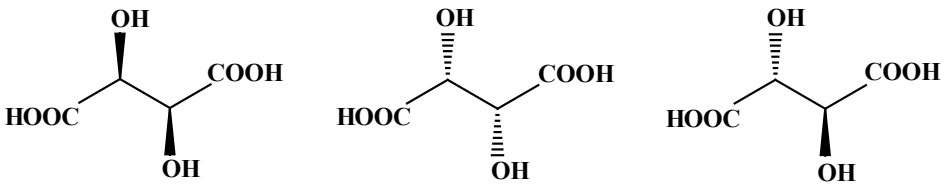

Figure 7.10: *Stereo formulas of the three isomers of tartaric acid.*

Molecule	CIP	Fischer	opt. rot.
Tartaric Acid	R,R	L	+
	S,S	D	−
	R,S	DL	0

Table 7.1: *Enantiomers of tartaric acid. Given are the CIP (R,S) nomenclature, the Fischer (D,L) nomenclature and the optical activity (+,−).*

The adsorption of tartaric acid on surfaces, especially the Cu(110) surface has long

been subject of interest. Several phases (see figure 7.11) have been identified and investigated[185, 239–241].

Table 7.2 shows the calculated chirality indices for all isomers of tartaric acid. It can easily be seen, that the two achiral isomers are absolutely indistinguishable from each other. es for all isomers of tartaric acid. It can easily be seen, that the two achiral isomers are absolutely indistinguishable from each other.

Molecule	Enantiomer	${}^{W}RCI$	${}^{V}RCI$	${}^{I}RCI$
tartaric acid	(R,R)	117861.0	596.88	528.43
	(S,S)	118915.0	604.38	531.42
	(R,S)	118389.2	600.64	529.93
	(S,R)	118389.2	600.64	529.93

Table 7.2: *Chirality indices RCI for tartaric acid according to Basak[218].*

Tartaric acid displays a very wide range of adsorption geometries on Cu(110)[185]. At least six different phases for sub-monolayer coverage have up to now been identified. Depending on substrate temperature and coverage different phases are predominately stable. Figure 7.11 gives an overview of the different phases. The phases actually investigated throughout this work are highlighted, the parameters used for preparation are given in table 7.3. In this work the two phases shown in figure 7.12 at (sub-)monolayer coverage were of major interest, namely the $c\,(4 \times 2)$-phase and the $(9\ 0|\pm 1\ 2)$-phase.

The adsorption of tartaric acid on copper takes place via a deprotonation of the carboxylic endgroup and covalent bonding of the two carboxy-oxygens to two adjacent copper atoms. At low substrate temperatures the molecules adsorb only via one carboxylic group forming monotartrate phases. For low coverages a centrosymmetric pattern is formed.

Phase	Substrate Temperature	Evaporation Temperature	Evaporation Time	Remarks
$\begin{pmatrix} 9 & 0 \\ \pm 1 & 2 \end{pmatrix}$	$330K$	$115°C$	$30s$	low coverage chiral phase
$c\,(4 \times 2)$	$305K$	$115°C$	$30s$	low coverage achiral phase
$\begin{pmatrix} 4 & \pm 1 \\ \pm 2 & 5 \end{pmatrix}$	$330K$	$115°C$	$600s$	high coverage chiral phase

Table 7.3: *Different Phases prepared with (R,R)-tartaric acid. (S,S)-tartaric acid leads to phases of opposite sign (opposite signs are given if needed).*

This $c\,(4 \times 2)$-phase is a monotartrate-phase, i.e. only one carboxylic group is deprotonated and bonds to the surface. The molecule is now oriented perpendicular to the surface

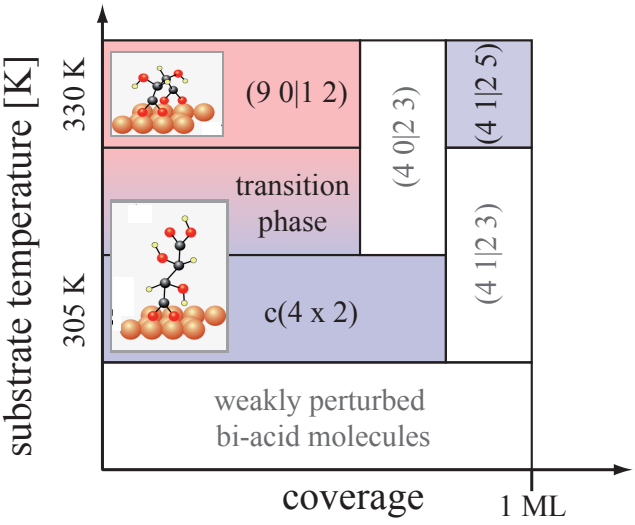

Figure 7.11: *Diagram of the adsorption phases of R,R-tartaric acid on Cu(110) in dependence on coverage and substrate temperature. All literature reported phases have been entered[185]. The phases under investigation here have been highlighted and adsorption models inserted where possible. Monotartrate phases are highlighted in blue, bitartrate phases in red.*

Phase	Substrate Temperature	Evaporation Temperature	Evaporation Time	Remarks
$\begin{pmatrix} 6 & \pm 1 \\ -1 & \pm 2 \end{pmatrix}$	$330K$	$115°C$	$30s$	low coverage chiral phase

Table 7.4: *Different Phases prepared with (R,S)-Tartaric Acid.*

and can be visualized as a circular shape, as can be seen in the STM-image in figure 7.12a. This does not allow for a certain ordering with respect to the copper lattice and results in a centered, i.e. achiral, phase. Upon increase of substrate temperature, either annealing after adsorption or keeping the substrate at higher temperature during adsorption (see table 7.3 for values), the $c\,(4 \times 2)$-phase is transformed into the $(9\ 0|\pm 1\ 2)$-phase.

Here, the second carboxylic group is also deprotonated and bound to the copper surface (i.e. a bitartrate phase), resulting in the oblong units displayed in figure 7.12b. Due to intermolecular interactions sketched in figure 7.14 involving the OH-groups, always three molecules combine to form long-range rows aligned along the $\langle 1\ \bar{1}\ 4 \rangle$-direction of the Cu surface[185, 188, 242]. Depending on the handedness of the molecule, this result in a $(9\ 0|-1\ 2)$ for R,R-Tartaric acid or $(9\ 0|1\ 2)$ for the S,S-enantiomer. In both cases the bonding takes place between both carboxylic O-atoms and two adjacent Cu-atoms in the Cu-rows of the (110) surface[242]. Upon further increase of coverage, the new molecules hydrate the already adsorbed molecules, i.e. one proton is transferred from a "new" to an "old" molecule, and all molecules arrange in a monotartrate pattern.

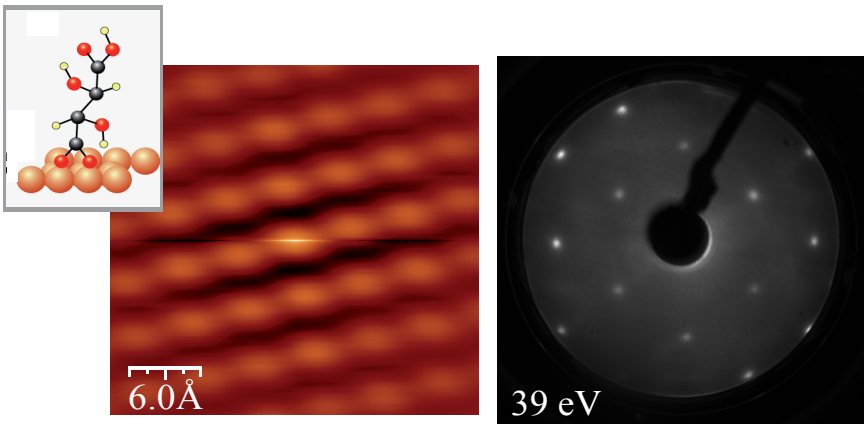

(a) $c\,(4 \times 2)$-*phase*

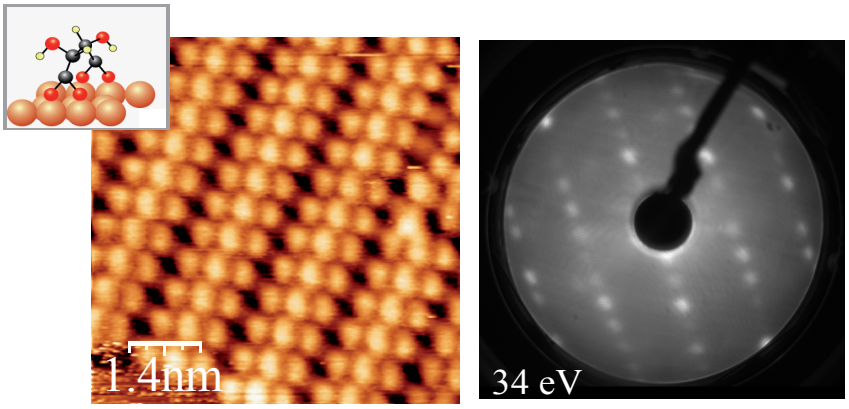

(b) $(9\ 0|\pm 1\ 2)$-*phase*

Figure 7.12: *The* $c\,(4 \times 2)$- *and* $(9\ 0|\pm 1\ 2)$-*phase under investigation in this work. Shown are STM-images and typical LEED patterns for these two phases. The insets show schematically the adsorption of the molecule to the surface. STM-images have been acquired myself at -1.63 V and -0.18 nA and -0.24 nA for the* $c\,(4 \times 2)$- *and*$(9\ 0|\pm 1\ 2)$-*phase, respectively.*

Apart from their chiral character, both phases, $c\,(4 \times 2)$ and $(9\ 0|\pm 1\ 2)$, do also differ in the way, the tartaric acid molecules adsorb to the surface, as the insets in figure 7.12 show.

The thermally induced decomposition of monoadsorbed tartaric acid into water, CO_2, carbon and hydrogen is catalysed by free surface sites. Since during decomposition new active sites are created, an autocatalytic process is induced. In the densely packed mono-tartrate form, the upper ends of the molecule cannot bend down and adsorb to the surface, a process that would inhibit the decomposition. Thus the decomposition takes place instantaneously and almost completely[240].

Both phases can be realised for the same coverage of tartaric acid, i.e. the same *number of*

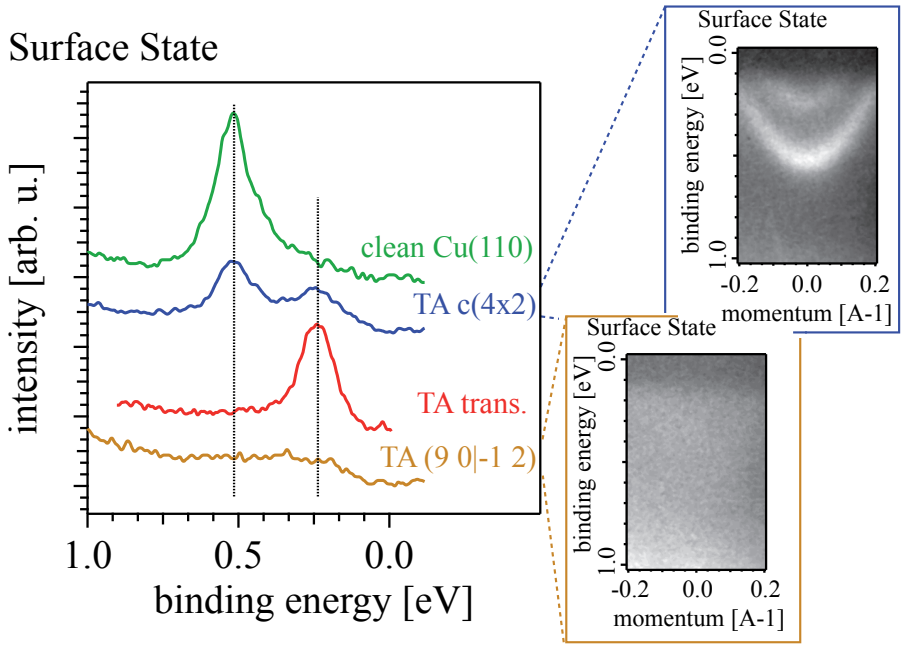

Figure 7.13: *The $c(4 \times 2)$- and $(9\ 0|\pm 1\ 2)$-phase under investigation in this work. Shown is the surface state of Cu(110) covered with tartaric acid acquired at 20 eV photon energy. The profiles show a cut through the center of the surface state. For the $c(4 \times 2)$- and $(9\ 0|\pm 1\ 2)$-phase the surface states are shown. Upon coverage with monotartrate the surface state is split. The original component vanishes upon transformation into the bitartrate phase. Upon full bitartrate coverage the surface state is completely vanished.*

molecules that are adsorbed onto the surface, and may thus serve as a nice model system to investigate the representation of ordering in the circular dichroism in the C1s core level emission. The actual coverage in terms of *covered substrate atoms* is not the same. In the monotartrate phase only one side of the molecules is bond to the surface, in the bitartrate phase both ends bond, spanning the space between two adjacent copper atom rows. Thus by means of covered atoms, the $(9\ 0|\pm 1\ 2)$bitartrate phase coverage is twice that of the $c(4 \times 2)$monotartrate phase.

This is nicely visible in the Cu(110) surface state, as seen at the bottom of figure 7.12. Upon adsorption of tartaric acid in the $c(4 \times 2)$-phase, the surface state loses intensity by about a factor of two, while a new parabola like state appears at 0.25 eV binding energy. The new state is of the same intensity as the decreased original surface state. This clearly indicates that the surface potential is altered upon the adsorption of tartaric acid, i.e. an electron transfer has taken place upon substrate-adsorbate-bond formation. The appearance of a gap state, which such a surface state indeed is, has already been observed for several kinds of adsorbates[42].

Subsequent annealing leads to a transition from the $c(4 \times 2)$- to the $(9\ 0|\pm 1\ 2)$-phase. During this transition, the second carboxylic group of the formerly singly bound mono-

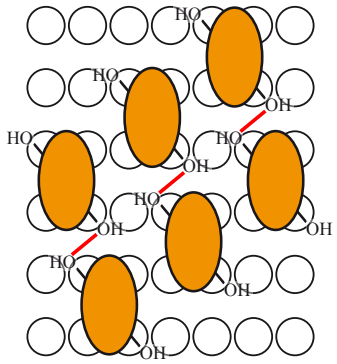

Figure 7.14: *Alignment of (S,S)-tartaric acid in the* $(9\ 0|\pm 1\ 2)$*-phase due to the OH-groups[188].*

tartrates is deprotoated for the molecules to bind to the surface in a bitartrate fashion. This can be observed nicely by the further decrease of the original surface state at 0.5 eV, which finally vanishes completely, and the further increase of the adsorbate-modified surface state at 0.25 eV (figure 7.13). Upon complete transformation, i.e. in the $(9\ 0|\pm 1\ 2)$-phase, at monolayer coverages all copper atoms are bound to molecules. Each molecule has four oxygen atoms, each bonding to a copper atom, thus a ratio of one-to-four molecules per copper atoms is achieved. In back conclusion this means that for the $c\,(4\times 2)$-phase only half of the copper atoms exhibit a bond to the adsorbate. In the completely covered $(9\ 0|\pm 1\ 2)$-phase the surface state vanishes completely. This can be seen in figure 7.13.

Although the basic bonding interaction, the bond between the two oxygens of the carboxylic group and two adjacent copper atoms, remains unchanged, the overall interaction between substrate and adsorbate is depending on the different adsorbate phases. And this interaction directly influences the electronic properties of the substrate. This could quite nicely be demonstrated through the Cu(100)-surface state.

The achiral meso-tartaric acid shows a similar adsorption behavior as its chiral companions. A mono- and a bitartrate layer can also be identified. But as the two chiral centers have opposite handedness, the hydroxy-ligands at those centers point in opposite directions and therefore the hydrogen bonds formed for adsorbate networks of the chiral species cannot be formed with the achiral species. The meso-bitartrate forms a $(6\ \pm 1|-1\ \pm 2)$ adlattice, i.e. two lattices of identical amount but opposite orientation are found on the surface. Upon coadsorption of $8mol\%$ of either one of the enantiomer, only the phase corresponding to the handedness of the coadsorbed species can be found[243]. A surface chirality has been induced in the system of adsorbed achiral molecules. The question remains, wether chirality has been induced only in the surface assembly or in the molecules themselves. In the latter case a way to easily produce truly chiral surfaces from achiral precursors would have been found. A method, specifically detecting the molecular chirality would be the tool needed, to reveal this question.

7.2.2 Spectral Asymmetry of adsorbed Chiral Tartaric Acid

The order of the molecules on the surface plays an important role for the investigation of chirality, as has widely been shown in the previous chapters.

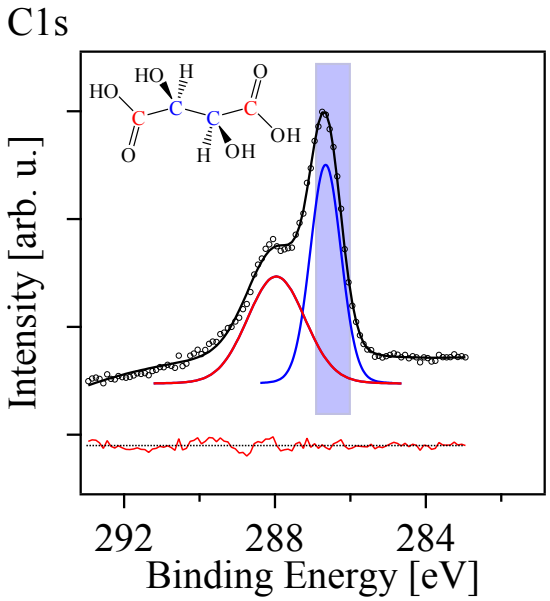

Figure 7.15: *C1s spectrum of tartaric acid in normal emission. Contributions of the different carbon atoms are color coded. The blue bar indicates the region of emission from the chiral centers, where a C1s-CD effect is supposed to be detected.*

Figure 7.15 shows a typical C1s core level spectrum of tartaric acid adsorbed to Cu(110) obtained at 380 eV photon energy. For the different adsorption phases either only one or both *COOH*-groups can be used for bonding. The latter case is shown here, but spectra for singly bonded tartaric acid is quite comparable, as the chemical shift of the non-bonded *COOH* does not vary much from the bonded one. At binding energies of 288 eV and 286.7 eV the emissions from the carboxylic groups and the chiral centers, respectively, can be detected.

C1s-CD plots have been taken for both enantiomers in both phases at comparable coverages. Cuts through the obtained asymmetry I_{ass} (see equation (7.39)) plots at the binding energy range indicated before in figure 7.15 are shown in figure 7.16. Due to the small differences in chemical environment for both chiral centers in the monotartrate $c\,(4 \times 2)$-phase, the area is shifted slightly to higher binding energies.

The asymmetry range in all four cases is similar with a maximum asymmetry of about $\pm 8\%$. In the case of the chiral phase absolute asymmetries are slightly larger than for the achiral phase. Figure 7.16 shows clearly that the asymmetry behavior for the (S,S)-enantiomer is opposite to the (R,R)-enantiomer. The (S,S)-enantiomer displays a positive asymmetry at negative emission angles and a negative asymmetry for positive emission

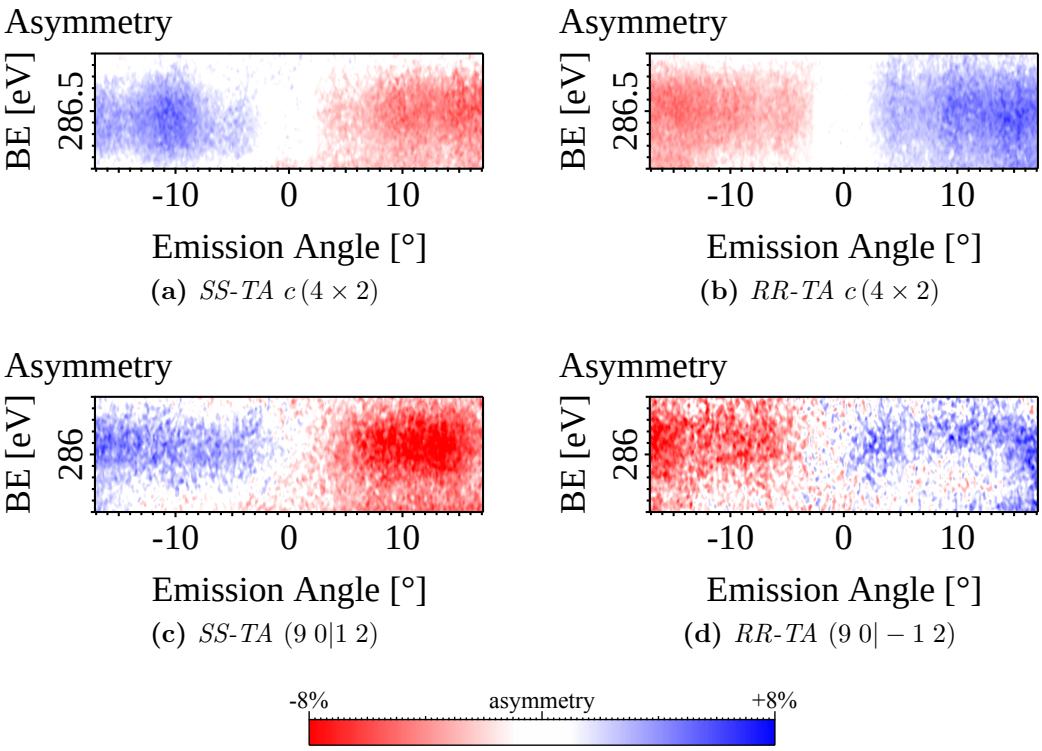

(a) *SS-TA* $c(4 \times 2)$ **(b)** *RR-TA* $c(4 \times 2)$

(c) *SS-TA* $(9\ 0|1\ 2)$ **(d)** *RR-TA* $(9\ 0|-1\ 2)$

Figure 7.16: *Asymmetry in the C1s core level emission of tartaric acid. Shown is the asymmetry in the emission from the chiral center for S,S- and R,R-tartaric acid (left and right, respectively). The top figures show the asymmetry observed for the* $(9\ 0|\pm 1\ 2)$*-phase, the bottom for the* $c(4 \times 2)$*-phase. Both phases show the same asymmetry-behavior: for the R-enantiomer a negative asymmetry for negative emission angles (and vice versa for the S-enantiomer).*

angles. The zero crossing appears exactly at normal emission.

For the achiral and chiral phases, the asymmetry plots are comparable. The overall behavior does not depend on the order of the molecule on the surface. This already gives rise to the assumption, that the C1s-CD is a measure for molecular chirality. The different absolute asymmetries might be explained by the different way of adsorption in achiral (monotartrate) and chiral (bitartrate) phase. In the bitartrate phase overall ordering of the molecules with respect to each other is higher due to intermolecular interactions mentioned before. Thus intramolecular ordering is also more rigid than in the monotartrate phase. Still these results clearly indicate that the ordering of the molecules on the surface does not determine the C1s-CD but the molecular chirality itself does.

The chirality indices in table 7.2 indicate a higher chirality for the (S,S)-enantiomer than the (R,R) one. But the ${}^{W}RCI$-value is only about $9\%_0$ larger than for the (R,R)-enantiomer. and thus too small to be detected in the C1s-CD-plots.

7.2.3 Achiral meso-tartaric acid

In comparison to the two chiral enantiomers (R,R) and (R,S) also the achiral (R,S)- or meso-tartaric acid has been investigated. Figure 7.17 shows the C1s-CD plot for a monolayer of (R,S)-tartaric acid on Cu(110). This displays no angle dependent asymmetry signal. On the one hand this is quite surprising, as also the (R,S)-tartaric acid is known to form enantiomorphous phases on the Cu(110) surface[243]. On the other hand, considering the results shown in figure 7.16, this could be expected. Nevertheless this result underlines the independence of the C1s-CD signal from the ordering on the surface.

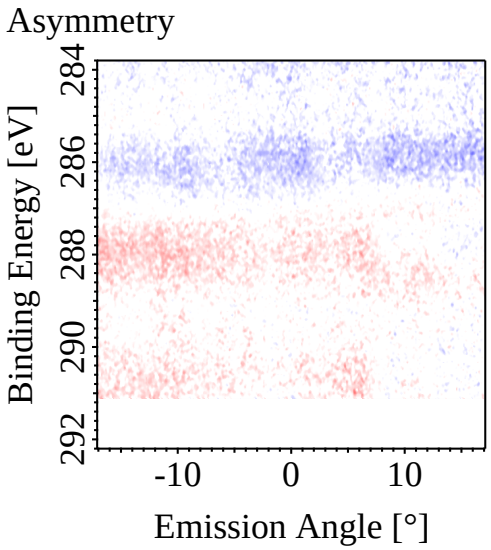

Figure 7.17: *Asymmetry in the C1s core level emission of achiral meso-tartaric acid. No asymmetry behavior can be detected.*

7.3 Chirality of Alanine and Cysteine

7.3.1 Adsorption phases of Alanine and Cysteine

The investigations on the appearance of chirality of tartaric acid gave rise to the assumption that the asymmetry in C1s core level emission might be an actual indicator for the chirality of the adsorbed molecule. Ordering of the adsorbates on the surface could be clearly ruled out. Still chirality within a molecule is present in the geometrical ordering of the ligands around a chiral center (described by the R,S-nomenclature) and in the physical property of optical activity (described by the +,−-notation). The historical Fischer-nomenclature is on the one hand an unambiguous geometrical description and on the other from its origin linked to the optical activity. Thus it may not be used as an ambiguous descriptor for chirality. Whether the observed asymmetry is governed by the optical activity or the actual geometry of the molecule could not finally be revealed. Therefore a model system of two molecules with one stereocenter had to be sought. While the stereocenters should be chemically (almost) identical, the correlation between geometry (R and S) and optical activity (+ and −) should be opposite. Ideally the overall molecules should not differ in size extremely much.

The amino acids alanine and cysteine appear to be an ideal model system. Alanine, classified as an aliphatic amino acid, is involved in several metabolic pathways. It can be synthesized by addition of hydrogen cyanide and ammonia to acetaldehyde following the Strecker reaction[244]. Cysteine, classified as a hydrophobic amino acid, works as an antioxidant and proteine linker. Due to its capability of metal complex formation it serves for various purposes in biological systems. It is used as a cigarette additive and may serve as hangover remedy. Currently cysteine is normally produced by hydrolysis of human hair.

As for all amino acids they posses an amine group (NH_2) and a carboxy group ($COOH$). Third ligand to the chiral center is a hydrogen atom (H). While the fourth ligand (subsequently denoted as end group) is a simple CH_3 group for alanine, cysteine has a CH_2SH end group.

The direct chemical environment of the chiral center is identical for both molecules (N, O, H and C from the endgroup) eliminating this as a possible source of influence on the C1s-CD. Still both amino acids exhibit an opposite optical activity. Due to its similarity of the chiral center both molecules may act as a proper test system to test the origin of the C1s-CD.

Alanine and cysteine bear only one stereocenter. Thus two enantiomers exist but no achiral form (see figure 7.18). The according Fischer nomenclature and optical rotation are given in table 7.5.

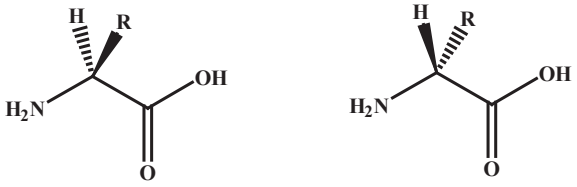

(S)-Enantiomer (R)-Enantiomer

Figure 7.18: *Stereo formulas of the two isomers of alanine and cysteine. The end group is denoted as R.*

Molecule	CIP	Fischer	opt. rot.
Alanine	R	D	−
	S	L	+
Cysteine	R	L	+
	S	D	−

Table 7.5: *Enantiomers of Alanine and Cysteine. Given are the CIP (R,S) nomenclature, the Fischer (D,L) nomenclature and the optical activity (+,−).*

Physical chemical properties are therefore also comparable for both molecules.

In table 7.3.1 the calculated chirality indices for all isomers of alanine and cysteine are reported. es for all isomers of alanine and cysteine are reported. Comparing the ${}^{W}RCI$ values with those of tartaric acid the chirality of alanine is only about 20% of tartaric acid, while cysteine is still about 60%. Again small differences between R and S isomer do exist but are still of a negligable dimension.

Molecule	Enantiomer	${}^{W}RCI$	${}^{V}RCI$	${}^{I}RCI$
alanine	R	23088	94.50	142.67
	S	22128	43.50	93.34
cysteine	R	69312	194.25	178.97
	S	69379	164.25	138.52

Table 7.6: *Chirality indices RCI for tartaric acid according to Basak[218].*
es RCI for tartaric acid according to Basak[218].

The adsorption of alanine especially on the Cu(110) surface has been widely studied, as well theoretically[245] an much more experimentally[185, 187, 235, 246].

Similar to tartaric acid several different adsorption phases are recognized for alanine (compare figure 7.19). They are determined if adsorption takes place solely via the carboxylic group or via carboxylic and amino group together. The bonding via the carboxylic group is proceeded via a deprotonation, thus the alanine can be regarded as anionic. In case of a second bond (via the amino group) the molecule is most likely to become zwitte-

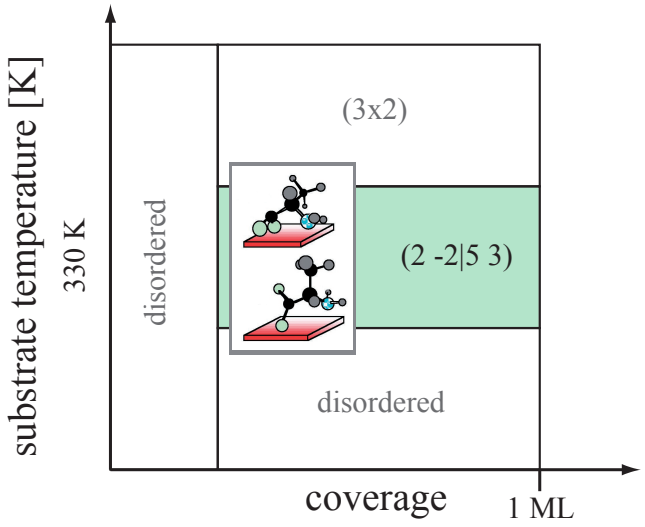

Figure 7.19: *Diagram of the adsorption phases of S-alanine on Cu(110) in dependence on coverage and substrate temperature. All literature reported phases have been entered[185]. The* $(2\ \pm 2|\mp 5\ 3)$*-phase under investigation here has been highlighted (green) and an adsorption model from literature[185] has been added.*

rionic. This work focused on the $(2\ \pm 2|\mp 5\ 3)$-phase, which was most reproducible in preparation. In this phase six to eight molecules form clusters that align along the $\left[\overline{1}\ 1\ 2\right]$ direction of the substrate lattice[187]. This phase has been described in detail by Raval and coworkers[186]. Within these clusters of six molecules three are bound by both functional groups while the other three are bound solely by one oxygen atom. Inbetween molecules of the same type hydrogen bonds between amino and carboxylic group are present, while hydrogen bonds between oxygen at the single-bond species and the hydrogens at the end-group of the double-bond species stabilize the clusters from within. Bonding to the surface takes place at the copper rows, four atoms and rows are spanned by one cluster in each direction.

Cysteine has three possible bonding sides. Besides the carboxylic and the amino group also the SH group is prone to deprotonation and bonding to a metal atom. Due to the high bonding affinity of sulfur to gold, the adsorption of cysteine on gold has been widely investigated[248–251]. There the molecules bond via the deprotonated thiol group and are present in the zwitterionic state[248].

Pradier and coworkers have investigated the adsorption of cysteine on Cu(110)[247]. For the deposition from the gas phase they propose an adsorption of zwitterionic cysteine molecules and bonding via the carboxylic and the thiol group. The determined core level spectra agree nicely with the spectra obtained in this work, such that it seems reasonable to assume the same bonding characteristics here. This results in a $(4\ \mp 1|\pm 1\ 5)$ordering of the molecules on the surface.

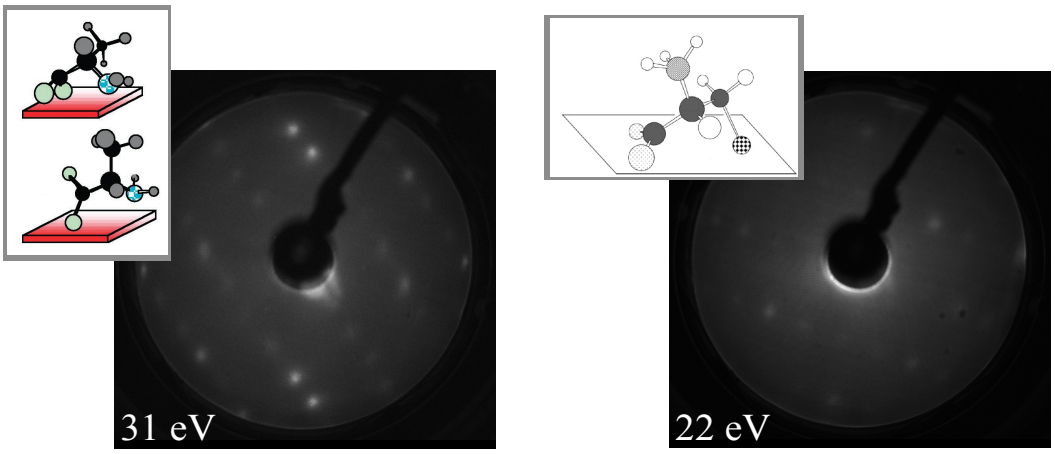

(a) *Alanine* $(2\ \pm 2|\mp 5\ 3)$ **(b)** *Cysteine* $(4\ \mp 1|\pm 1\ 5)$

Figure 7.20: *The* $(2\ \pm 2|\mp 5\ 3)$*- and* $(4\ \mp 1|\pm 1\ 5)$*-phase under investigation in this work. Shown are and typical LEED patterns for these two phases. The insets show schematically the adsorption of the molecules to the surface[186, 247].*

7.3.2 Asymmetry dependence - structure or optical activity?

Especially the chirality and the spectral behavior of alanine has been investigated in recent years. Following calculations by Powis predicting a CDAD effect detectable for alanine[252] Woodruff and coworkers investigated the CDAD of alanine adsorbed on Cu(110)[235, 246]. They could detect a very weak CDAD signal that they assigned to the molecular chirality. It should be noted that the zero crossing was few degrees off normal emission. Still they regard this effect to be too weak for actual application.

The experiments on tartaric acid have shown that the asymmetry is independent of the adsorption geometry of the molecule. Thus the totally different order for alanine and cysteine are not supposed to influence the C1s-CD measurements. Therefore only the two previously mentioned phases will be shown here. Exemplary spectra of other phases reveal no differences from these results.

Figure 7.21 shows the C1s spectra of both molecules adsorbed on Cu(110). Both spectra exhibit three components, which can be attributed to the three carbon atoms, at binding energies of 288.4 eV, 286.35 eV and 285.75 eV. Shifts to 0.8 eV lower binding energies in the C1s spectra of cysteine are due to the sulfur atom in the endgroup. The emission from the endgroup is shifted by about 1 eV. These core level spectra agree nicely with the C1s spectra obtained by Umbach and coworkers for crystalline amino acids[163]. These authors detect a strong decomposition upon x-ray irradiation. Using the ability to detune the undulator and reduce the flux density on the sample, this effect has been prevented in this work. Permanent observation of the core levels and valence band structures ensured

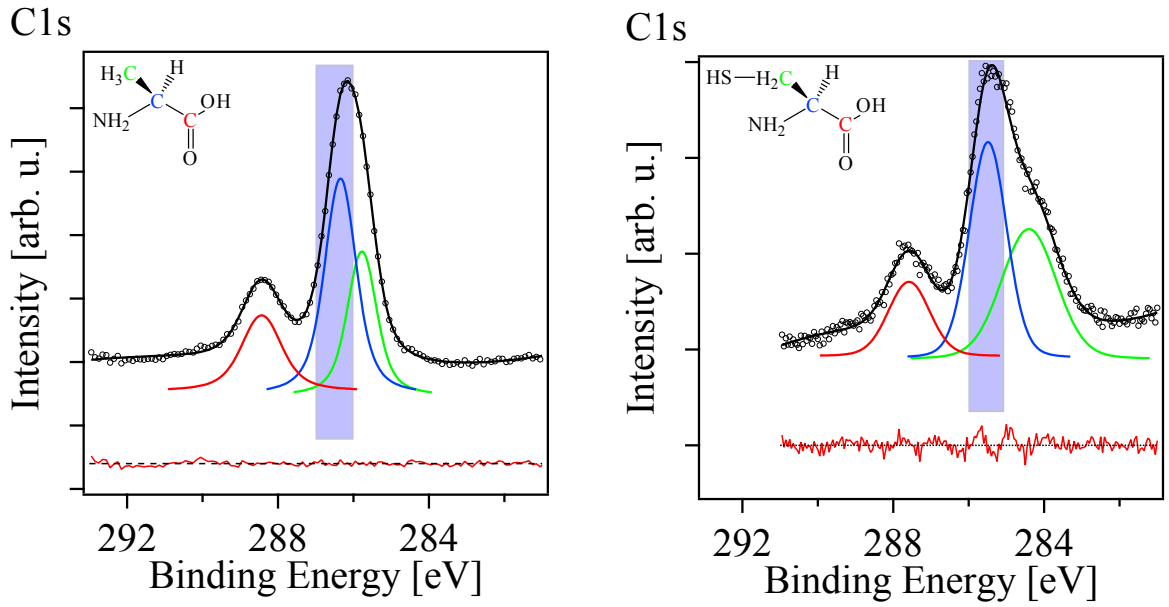

(a) *Alanine* **(b)** *Cysteine*

Figure 7.21: *C1s spectra of alanine and cysteine in normal emission. Contributions of the different carbon atoms are color coded. The blue bar indicates the region of emission from the chiral centers, where a C1s-CD effect is supposed to be detected.*

the prevention of beam damage.

Figure 7.22 shows the asymmetry in the C1s core level emission within the energy range indicated in figure 7.21. The maximum asymmetry is ±3%, this corresponds to only 1/3 of the asymmetry observed for tartaric acid. This corresponds on a qualitative scale to the different chirality indicees of the molecules. The spectra for alanine display a well observable asymmetry behavior, which corresponds to the behavior of tartaric acid, except that zero crossing is moved about $-3°$ to $-5°$ off normal emission. The reason for this shift may be sought in the diffraction of the photoelectrons in the molecules. But a confirmation of this assumption would need further experimental investigations.

For cysteine this behavior is less well observable, the zero crossing not clearly identifiable. Still the overall trend is clear and unambiguous. The comparison between the asymmetry in the C1s emission from different alanine and cysteine isomers shows a clear dependence of this asymmetry on the handedness of the stereocenters of the molecules under investigation.

For either two spectra shown in figure 7.22 adsorption interaction (via oxygen, nitrogen or sulfur), ordering on the surface ((2 $\pm$ 2| $\mp$ 5 3)or (4 $\mp$ 1| $\pm$ 1 5)) and optical activity are different. Still both R-enantiomers and both S-enantiomers observe the same asymmetry plot - and the same asymmetry plot the R- and S-enantiomers of tartaric acid have shown.

This now very clearly indicates, that only the geometrical structure of the adsorbate, i.e.

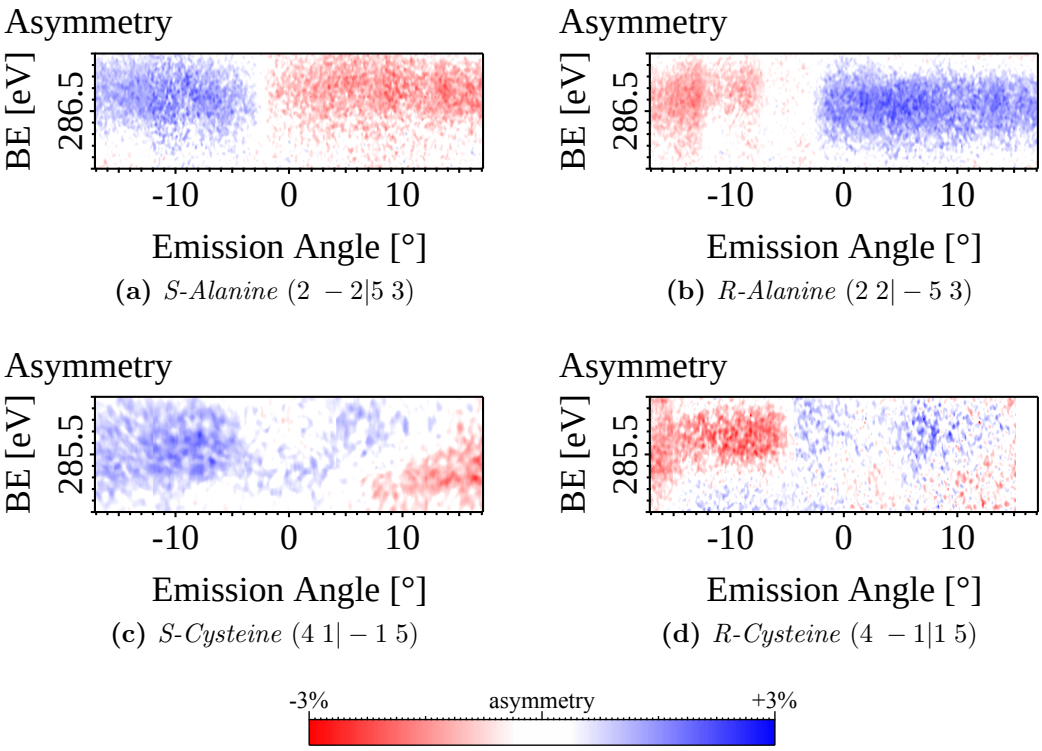

(a) *S-Alanine* $(2\ -2|5\ 3)$ **(b)** *R-Alanine* $(2\ 2|-5\ 3)$

(c) *S-Cysteine* $(4\ 1|-1\ 5)$ **(d)** *R-Cysteine* $(4\ -1|1\ 5)$

Figure 7.22: *Asymmetry in the C1s core level emission of S- and R-Alanine (7.22a and 7.22b) and S- and R-Cysteine (7.22c and 7.22d), respectively. Displayed is the asymmetry in the emission from the chiral center. Both molecules show for the R-enantiomer a negative asymmetry for negative emission angles (and vice versa for the S-enantiomer). The maximum asymmetry is ±3%. For alanine, the zero crossing is moved by about -3° to -5° off normal emission. For cysteine the zero crossing seems also to be shifted, the shift cannot be clearly quantified.*

whether R or S, is determining the asymmetry of the C1s core level emission.

7.3.3 At the edge of measurement - technical difficulties

While the asymmetry plots for tartaric acid are clearly unambiguous, for alanine and cysteine they are not as good. Though the overall trend is still well visible, details as the exact zero crossing point cannot be determined any more. A look on the complete asymmetry plots in figure 7.23 of cysteine reveal the problems.

The obtained spectra and therefore the obtained asymmetries are in comparison to e.g. the tartaric acid data very noisy and susceptible to spikes at the overlap regions of the spectral slabs. Every single spectrum shown here for cysteine has been acquired for about one hour, thus the whole asymmetry plot requires about one twelve-hour BESSY shift. Therefore the quality shown here can be assumed to be the optimum currently obtainable. From

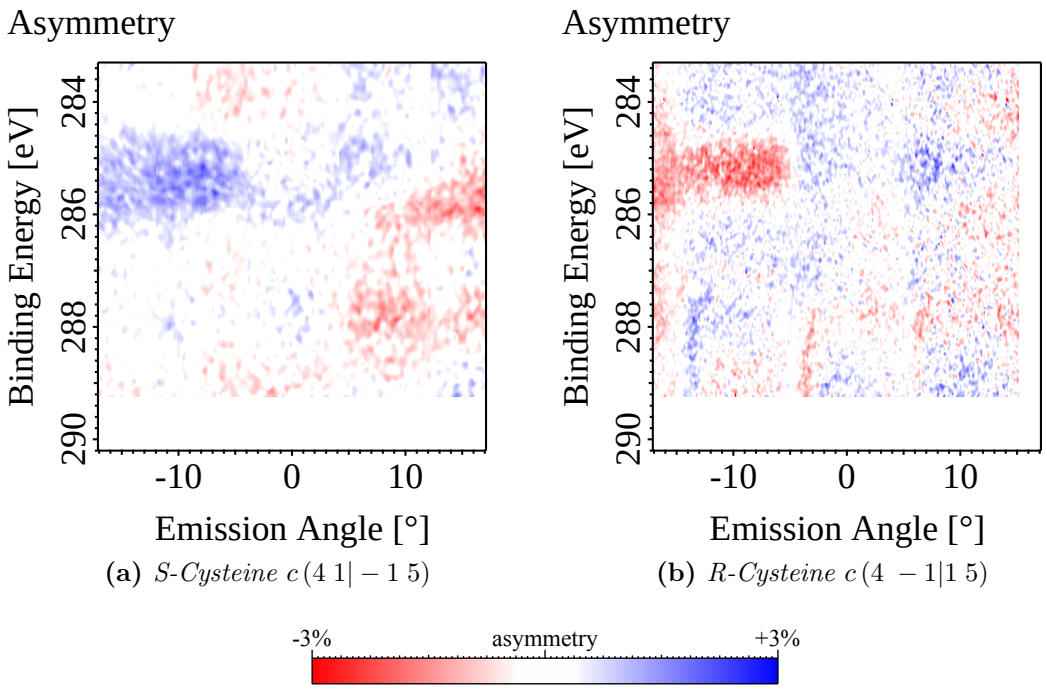

(a) *S-Cysteine* $c\,(4\ 1|-1\ 5)$ **(b)** *R-Cysteine* $c\,(4\ -1|1\ 5)$

Figure 7.23: *Asymmetry of S- and R-cysteine on Cu(110). The same spectra are shown as in figure 7.22 but now over the whole energy range of the C1s emission. The high noise level is clearly observable, making the interpretation of the cysteine data difficult.*

this point of view the utilization of the circular dichroism has its limitations here - which are pushed much further than expected by Woodruff and coworkers not long ago[246]. Not to mention the problems that might arise through such long exposure times, such as beam damage, beam instabilities, and so forth. At this point it seems, that this technique may only find a well application for molecules of high chirality index.

7.4 Chirality in Photoemission

C1s-CD spectra for different molecules have been acquired. These molecules observed different adsorption behavior, i.e. bonding to the surface took place via various atoms, the intermolecular interactions varied from molecule to molecule and thereby the short- and long range order of the molecules on the surface. The molecules exhibited different optical activity of different strength and posses different strong chirality expressed by the chirality index.

Despite all differences, the behavior of asymmetry in the C1s emission followed the mere geometrical structure at the stereocenter(s). It can thus be assumed as a technique to access substrate independently the molecular chirality. For molecules with a right handed stereocenter the asymmetry was negative at emission angles negative to normal emission and positive for angles positive to normal emission. Molecules with a left handed stereocenter observed the opposite behavior. This makes this method highly advantageous to CDAD, where an asymmetry also can be detected but no direct conclusion from its sign to the chirality of the molecule can be made. On a qualitative scale the predictions of the *RCI* chirality index can be approved. For a quantitative comparison better experimental data would be needed.

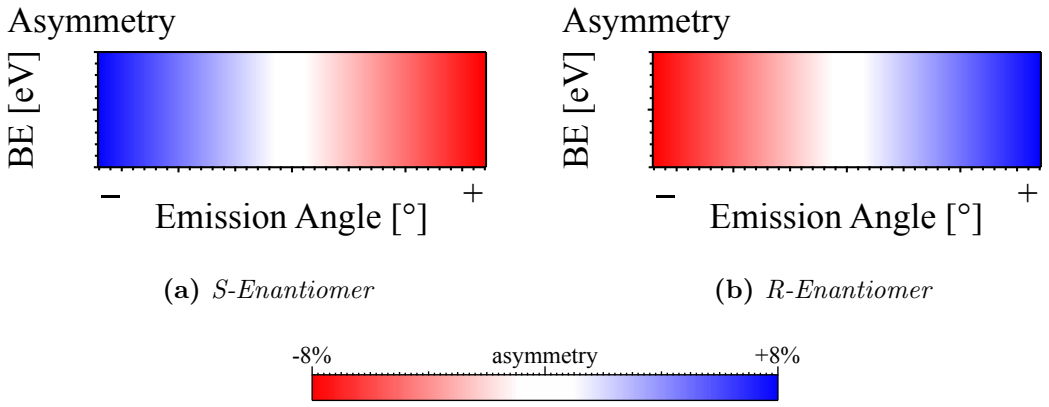

(a) *S-Enantiomer* **(b)** *R-Enantiomer*

Figure 7.24: *Negative Asymmetry at negative emission angles describes the R-Enantiomer. Positive Asymmetry at positive emission angles describes the S-Enantiomer.*

The asymmetry in the C1s core level emission from a chiral molecule is a qualitative indicator and unambiguous identifier of the molecular chirality according to the CIP-rules: *Negative* Asymmetry at *negative* emission angles describes the *R*-Enantiomer. Positive Asymmetry at negative emission angles describes the S-Enantiomer.